AGU PUBLICATIONS

Geophysical Research Letters

RESEARCH LETTER
10.1002/2016GL072430

Key Points:
- Model skill of the Maritime Continent (MC) winter mean low-level moisture pattern is highly correlated with MJO eastward propagation skill
- The amplitude of MC mean low-level moisture is greatly underestimated in poor MJO models, leading to discrepancies in moisture advection
- The seasonal mean lower level moisture pattern over the MC is a useful diagnostic metric to evaluate MJO propagation in climate models

Correspondence to:
A. O. Gonzalez,
alex.o.gonzalez@jpl.nasa.gov

Citation:
Gonzalez, A. O., and X. Jiang (2017), Winter mean lower tropospheric moisture over the Maritime Continent as a climate model diagnostic metric for the propagation of the Madden-Julian oscillation, *Geophys. Res. Lett.*, *44*, 2588–2596, doi:10.1002/2016GL072430.

Received 22 DEC 2016
Accepted 21 FEB 2017
Accepted article online 23 FEB 2017
Published online 11 MAR 2017

Winter mean lower tropospheric moisture over the Maritime Continent as a climate model diagnostic metric for the propagation of the Madden-Julian oscillation

Alex O. Gonzalez[1,2] **and Xianan Jiang**[1,2]

[1]Joint Institute for Regional Earth System Science and Engineering, University of California, Los Angeles, California, USA, [2]Jet Propulsion Laboratory, California Institute of Technology, Pasadena, California, USA

Abstract Despite its widespread influences on the atmosphere, the Madden-Julian oscillation (MJO) remains poorly represented in state-of-the-art general circulation models (GCMs). Motivated by recent findings that the horizontal advection of the mean low-tropospheric moist static energy or moisture by the MJO winds plays a crucial role in the eastward propagation of the MJO, we investigate the relationship between lower tropospheric moisture patterns over the Indo-Pacific and MJO eastward propagation in a suite of 23 GCM simulations. Model capability of reproducing the observed November–April mean lower tropospheric moisture pattern over the Indo-Pacific, especially near the Maritime Continent (MC), is highly correlated with model skill in simulating MJO eastward propagation. In GCMs with difficulty capturing realistic MJO propagation, the amplitude of the mean low-level moisture over the MC is greatly underestimated, leading to weak horizontal moisture gradients and thus discrepancies in moisture advection, significantly affecting MJO propagation. This study suggests that the mean lower tropospheric moisture pattern over the MC can serve as an important diagnostic metric for MJO propagation in climate models.

1. Introduction

The Madden-Julian oscillation (MJO) [*Madden and Julian,* 1971, 1972] is a planetary-scale tropical atmospheric disturbance with an intraseasonal time scale of 30–90 days. MJO convection often initiates in the western equatorial Indian Ocean and slowly propagates eastward along the equator at about 5 m s^{-1}. During its eastward movement, the MJO exerts significant modulations on a myriad of atmospheric weather and climate phenomena, such as El Niño–Southern Oscillation, global monsoons, tropical cyclones, and extratropical weather extremes (see a recent review by *Zhang* [2013]). Meanwhile, the MJO is thought to be one of primary sources of predictability for extended-range weather prediction [*Ferranti et al.*, 1990; *Hurrell et al.*, 2009; *Waliser et al.*, 2012; *Vitart et al.*, 2012; *Neena et al.*, 2014; *NAS*, 2016].

Various mechanisms have been put forth to interpret the essential characteristics of the observed MJO [*Zhang*, 2005; *Wang*, 2012]. However, a comprehensive MJO theory remains elusive. Recent studies have adopted the "moisture mode" concept to improve understanding of instability and propagation mechanisms associated with the MJO [e.g., *Raymond and Fuchs*, 2009; *Sobel and Maloney,* 2012, 2013; *Pritchard and Bretherton*, 2014; *Adames and Kim*, 2016; *Jiang et al.*, 2016; *Jiang,* 2017]. Within the moisture mode paradigm, MJO precipitation is mainly regulated by column moisture (i.e., precipitable water) perturbations, which can be linked to column moist static energy (MSE) under weak-temperature gradient theory over the Indo-Pacific warm pool where the MJO is most active. To this end, MSE processes have been comprehensively examined using both observations and model simulations to identify key MJO physics [e.g., *Maloney*, 2009; *Kiranmayi and Maloney*, 2011; *Andersen and Kuang*, 2012; *Kim et al.*, 2014; *Sobel et al.*, 2014; *Arnold and Randall*, 2015; *Jiang et al.*, 2016; *Wolding et al.*, 2016; *Jiang,* 2017].

While cloud-radiation and surface wind-evaporation feedbacks tend to play a critical role in destabilizing the MJO [e.g., *Raymond*, 2000; *Maloney and Sobel*, 2004; *Sobel et al.*, 2010; *Andersen and Kuang*, 2012; *Sobel et al.*, 2014; *Wolding et al.*, 2016], column-integrated MSE advection, particularly its horizontal component, is considered to be essential in driving the eastward propagation of the MJO [e.g., *Maloney*, 2009; *Kiranmayi and Maloney*, 2011; *Andersen and Kuang*, 2012; *Pritchard and Bretherton*, 2014; *Kim et al.*, 2014; *Sobel et al.*, 2014;

Arnold and Randall, 2015]. With a partial contribution from high-frequency eddy transport [*Maloney and Dickinson*, 2003; *Maloney*, 2009; *Kiranmayi and Maloney*, 2011; *Andersen and Kuang*, 2012; *Benedict et al*., 2015], total horizontal MSE advection associated with the MJO is largely dominated by the advection of the seasonal mean MSE by MJO wind anomalies [e.g., *Kiranmayi and Maloney*, 2011; *Kim et al*., 2014]. The importance of mean MSE advection by the MJO circulation in MJO propagation has been further confirmed by a recent analysis based on multimodel simulations from the MJO Task Force (MJOTF) and the Global Energy and Water Cycle Experiment Atmospheric System Study (GASS) MJO model comparison project [*Jiang,* 2017]. *Jiang* [2017] shows that in GCMs that poorly represent the eastward propagation of the MJO, significant model deficiencies are noted in both lower tropospheric (mainly between 400 and 900 hPa) mean MSE pattern and MJO circulations, leading to rather weak positive (negative) MSE tendencies to the east (west) of MJO convection.

Since MSE is largely dominated by the moisture field in the lower troposphere, the role of horizontal moisture advection, specifically advection of mean moisture by the MJO anomalous winds, in the eastward propagation of the MJO has also been confirmed by both observations and model simulations [e.g., *Hsu and Li*, 2012; *Cai et al*., 2013; *Chikira*, 2014; *Adames and Wallace*, 2015; *Nasuno et al*., 2015; *Wolding et al*., 2016]. These results thus indicate that realistic model representation of the lower tropospheric mean moisture pattern over the Indo-Pacific region could be critical to faithfully simulate the eastward propagation of the MJO.

Motivated by these previous studies, we analyze multimodel simulations from more than 20 GCMs participating in the recent MJOTF/GASS MJO project [*Petch et al*., 2011; *Klingaman et al*., 2015; *Jiang et al*., 2015] and examine the relationship between model skill in simulating MJO eastward propagation and the November–April mean lower tropospheric moisture pattern. Significant correlations between model skill of the eastward propagation of the MJO and low-level mean moisture pattern over the Indo-Pacific region are evident. In particular, we pinpoint a region near the Maritime Continent (MC) where the model mean low-level moisture pattern is highly correlated with model MJO eastward propagation.

2. Data Set and Methods

The multimodel data set used for this study is from the climate simulation component of the MJOTF/GASS MJO global model comparison project. We analyze 23 simulations based on 21 GCMs due to the availability of three-dimensional specific humidity fields (see Table A1 in Appendix A for details of these models). All of the participating models were integrated for 20 years, either with atmosphere-ocean coupling or with an atmosphere-only setting forced by the observed sea surface temperatures and sea ice concentrations during the period of 1991–2010. Output was archived every 6 h on standard horizontal ($2.5° \times 2.5°$) grids and 22 vertical pressure levels. For details of this data set, please refer to *Jiang et al.* [2015]. The Tropical Rainfall Measuring Mission (TRMM)-based rainfall estimates (version 3B42 v7) [*Huffman et al*., 2007] as well as the European Centre for Medium-Range Weather Forecasts ERA-Interim reanalysis [*Dee et al*., 2011] for the 15 year period of 1998–2012 are used to validate the model simulations.

Following *Jiang et al.* [2015, Figures 3 and 4] and *Jiang* [2017, Figure 1], MJO propagation skill in each GCM is measured by pattern correlations of simulated anomalous rainfall Hovmöller (time-longitude) diagrams, derived by lag regressions of intraseasonally (20–100 day) filtered rainfall onto averaged values over an Indian Ocean and a western Pacific base point, against their TRMM counterparts. Six GCMs with the highest MJO propagation skill are then identified as the "good" MJO models (GISS-E2, ECHAM5-SIT, CNRM-CM, SPCCSM3, MRI-AGCM3, and ECEarth3), and six other GCMs with the lowest skill as the "poor" MJO models (CWB-GFS, CanCM4, MIROC5, ISUGCM, CFSv2, and NavGEM1). Analyses in this study focus on the extended boreal winter season, November–April (hereafter just referred to as the winter season for brevity).

3. Results

Figure 1a illustrates spatial distributions of the winter mean lower tropospheric (650–900 hPa) specific humidity over the Indo-Pacific region based on ERA-Interim reanalysis. The ERA-Interim low-level mean moisture pattern is characterized by a moisture maximum over the MC near 140°E. As previously mentioned, a strong horizontal gradient associated with this low-level mean moisture pattern, with

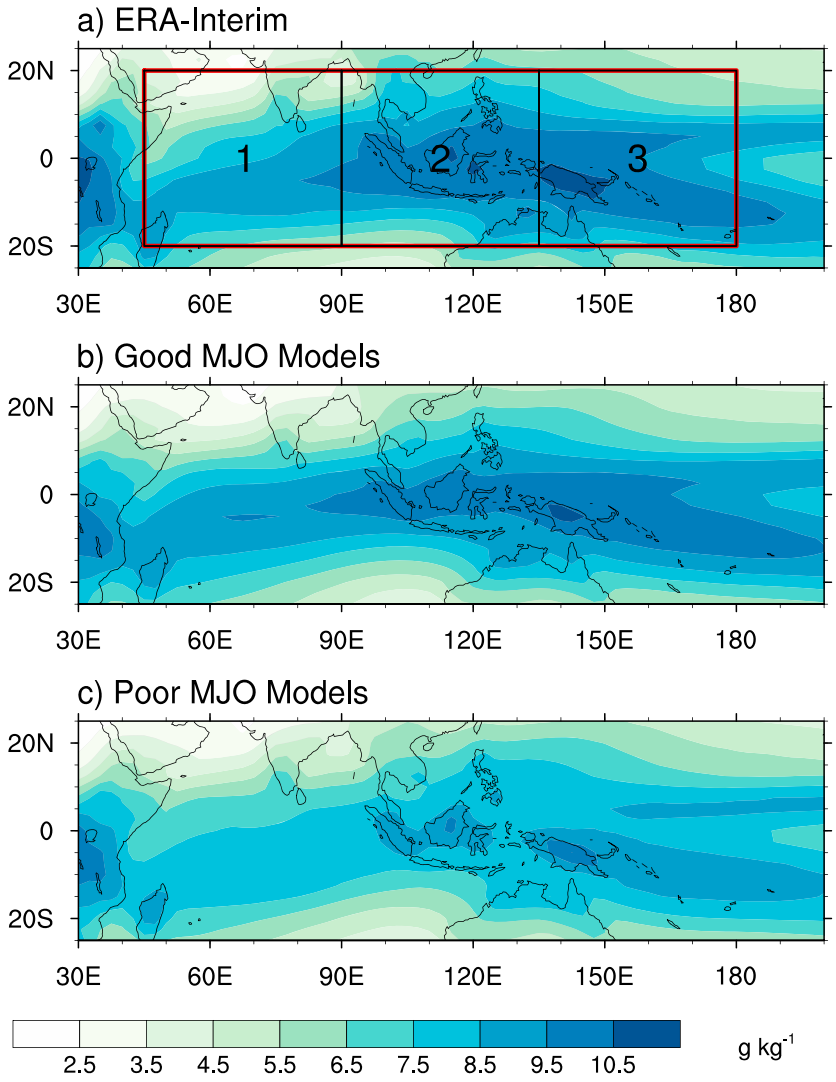

Figure 1. The winter (November–April) mean specific humidity (g kg^{-1}) averaged over 650–900 hPa for (a) ERA-Interim, (b) the good MJO models, and (c) the poor MJO models. The good and poor MJO models are defined using a lag-regression method discussed in section 2. Four regions are highlighted, three in the thin black boxes: (1) Indian Ocean (20°S–20°N, 45°E–90°E), (2) MC (20°–20°N, 90°E–135°E), and (3) west Pacific Ocean (20°S–20°N, 135°E–180°E), and a fourth broader region denoted as the Indo-Pacific region (20°S–20°N, 45°E–180°E) in the thick red line.

Table 1. Correlation Coefficients Between Mean Moisture Pattern Skill and MJO Propagation Skill[a]

Regions	Correlation Between Model Skill of Mean Moisture Pattern and MJO Propagation
Indian Ocean (45°E–90°E, 20°S–20°N)	0.54
Maritime Continent (90°E–135°E, 20°S–20°N)	**0.80**
West Pacific Ocean (135°E–180°E, 20°S–20°N)	0.23
Indo-Pacific (45°E–180°E, 20°S–20°N)	0.53

[a]Correlation coefficients between model skill in representing the winter mean specific humidity and MJO propagation over the Indo-Pacific regions defined in Figure 1. Model skill for low-level moisture patterns in each model is defined by the pattern correlation between the model-simulated and ERA-Interim reanalysis 650–900 hPa averaged winter mean specific humidity pattern. Model skill for MJO propagation is determined by individual model lag-regressed time-longitude rainfall evolution diagrams correlated against their TRMM counterparts. Note the high correlation between MJO propagation skill and mean moisture pattern skill over the Maritime Continent (in bold font for clarity).

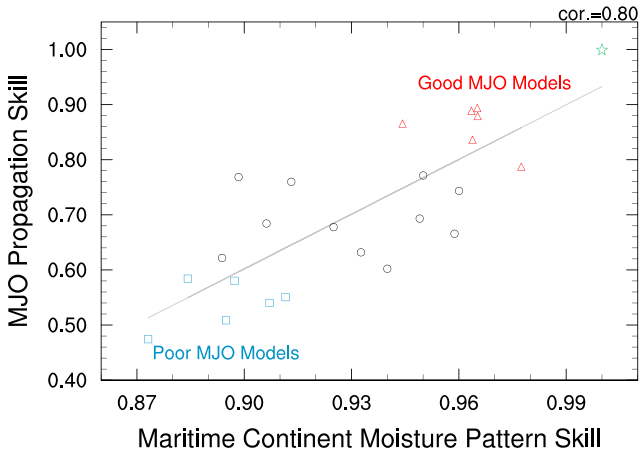

Figure 2. Scatterplot between model skill in representing the 650–900 hPa averaged winter mean specific humidity over the MC (90°E–135°, 20°S–20°N) and MJO propagation skill. The red triangles and blue boxes represent the good and poor models of MJO propagation, respectively. TRMM MJO propagation skill and ERA-Interim MC moisture pattern skill are denoted by the green star. A linear best fit regression line by least squares means is shown in the gray line, and the correlation coefficient is shown in the top right corner.

decreasing amplitude westward along the equator and poleward on both sides of the equator, is essential for the eastward propagation of the MJO over the Indo-Pacific region [*Hsu and Li*, 2012; *Nasuno et al.*, 2015; *Adames and Wallace*, 2015]. This is further supported by the realistically simulated mean moisture pattern in the good MJO models (Figure 1b) in accordance with strong eastward MJO propagation in these models. In contrast, the moisture maximum over the MC and thus horizontal gradient are largely underestimated in the poor MJO models (Figure 1c) along with their rather weak MJO eastward propagation. The low-level mean moisture pattern in the poor MJO models largely resembles the low-level MSE pattern in *Jiang* [2017], suggesting that the largely underestimated horizontal MSE (moisture) advection is responsible for weak MJO eastward propagation in these models.

We further examine how model skill in representing the low-level mean moisture pattern over the Indo-Pacific is related to model MJO eastward propagation across the 23 model simulations. Model skill for the low-level moisture pattern in each model is defined by the pattern correlation between the model-simulated and ERA-Interim reanalysis (shown in Figure 1a) 650–900 hPa averaged winter mean moisture pattern. Model skill for MJO propagation is determined by individual model lag-regressed time-longitude rainfall evolution diagrams correlated against their TRMM counterparts, as discussed in section 2. Table 1 illustrates correlation coefficients between MJO propagation skill and model skill of the winter mean 650–900 hPa specific humidity pattern over the three subregions along with the entire Indo-Pacific domain shown Figure 1a. The three subregions are denoted as the (1) Indian Ocean (20°S–20°N, 45°E–90°E), (2) MC (20°S–20°N, 90°E–135°E), and (3) west Pacific Ocean (20°S–20°N, 135°E–180°E). Note that slight changes of each domain size do not significantly

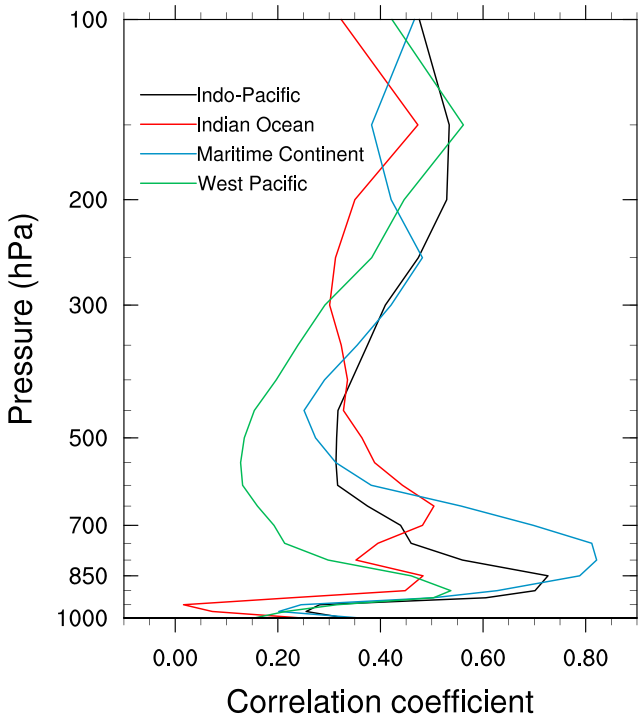

Figure 3. Correlation coefficients between model MJO propagation skill and model skill in representing the winter mean specific humidity pattern at each vertical level between 1000 and 100 hPa over the four regions defined in Figure 1 across 23 GCM simulations.

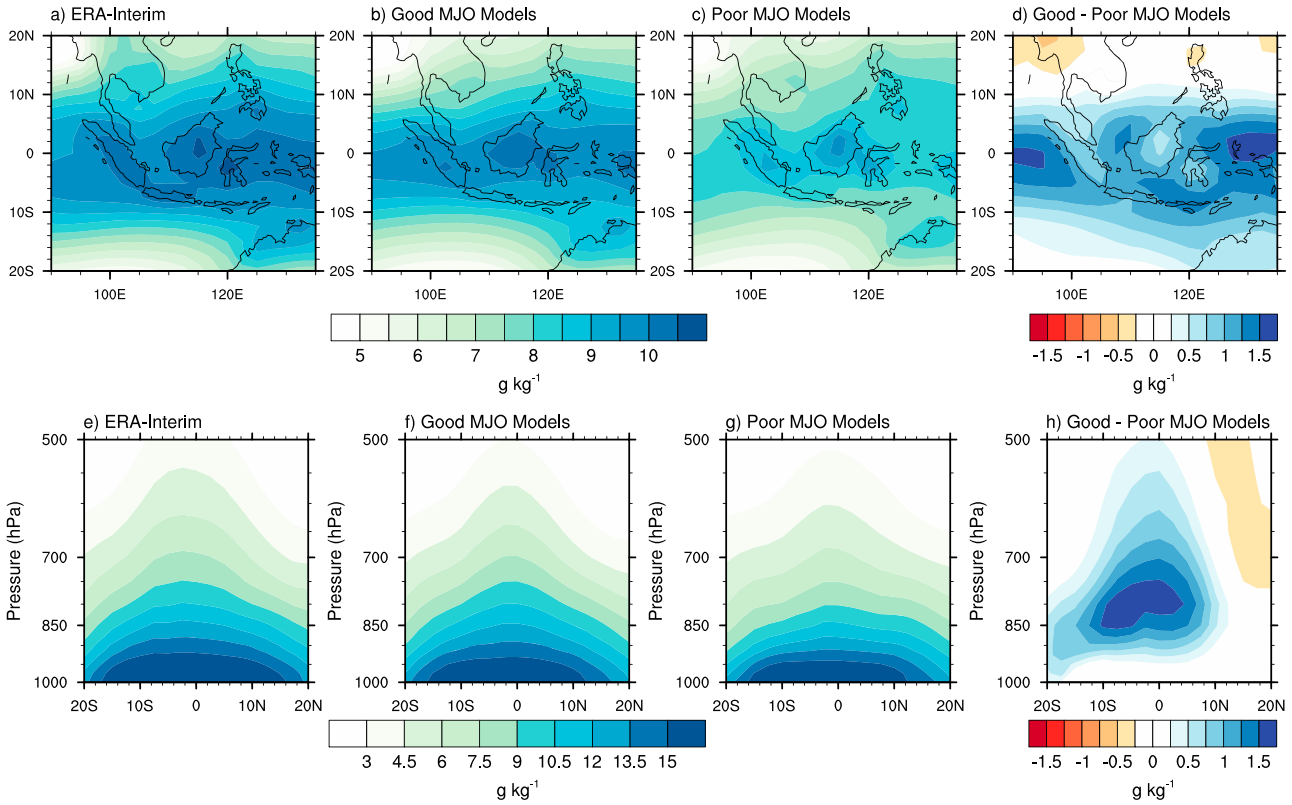

Figure 4. The winter mean 650–900 hPa averaged specific humidity (g kg^{-1}) in the MC region for (a) ERA-Interim, (b) the good MJO models, (c) the poor MJO models, and (d) the difference between the good and poor MJO models. The panels in Figures 4e–4h are latitude-vertical profiles of winter mean specific humidity averaged over the MC longtitudes (90°E–135°E) for (e) ERA-Interim, (f) the good MJO models, (g) the poor MJO models, and (h) the difference between the good and poor MJO models. Contour intervals are 0.5 g kg^{-1} in Figures 4a–4c, 1.5 g kg^{-1} in 4e–4g, and 0.3 g kg^{-1} in 4d and 4h, respectively.

change the correlations. Also, the selection of the MC region in Figure 1a is adjusted to maximize the correlation coefficient.

A high correlation of 0.53 (at the 99.5% significance level) between model skill in representing the winter mean low-level moisture pattern over the broad Indo-Pacific region and MJO propagation skill is indeed discerned across the 23 GCM simulations, confirming the aforementioned notion that the mean low-level moisture distribution in the Indo-Pacific region is critical to accurately simulate the eastward propagation of the MJO. While similar correlations between model MJO propagation skill and model skill in simulating mean moisture patterns over the Indian Ocean subdomain are also observed, the mean moisture pattern over the west Pacific is not significantly correlated with MJO propagation. Particularly noteworthy is the MC region, where a very high correlation (0.8) is found between the winter mean moisture pattern skill and MJO propagation skill, suggesting that the realistic simulation of the mean moisture distribution over the MC could be vital to realistically simulate MJO eastward propagation in GCMs.

As further shown in Figure 2, GCMs that realistically capture the eastward propagation of the MJO also tend to accurately simulate the 650–900 hPa mean moisture pattern over the MC (red triangles), and vice versa for the poor MJO models (blue boxes). In addition to the correlation coefficients between MJO propagation skill and the 650–900 hPa vertically averaged moisture pattern skill, similar correlation coefficients between MJO propagation skill and model skill in representing the winter moisture pattern at each vertical level between 1000 and 100 hPa over the four Indo-Pacific domains are further displayed in Figure 3. The results clearly indicate that mean moisture patterns in the lower troposphere are best correlated to MJO eastward propagation, justifying our selection of vertical levels between 650 and 900 hPa for deriving the mean lower tropospheric vertically averaged moisture pattern. It is worth noting that the model moisture patterns near the boundary layer (below 900 hPa) do not show a close association with MJO propagation in the multimodel simulations. This result is consistent with previous findings from MJO MSE diagnoses based on observations [*Kim et al.*,

2014], and the general relationship between tropical rainfall variability and vertical specific humidity profiles [*Holloway and Neelin*, 2009].

Figures 4a–4d further show the detailed spatial maps of the winter mean 650–900 hPa averaged specific humidity over the MC region for ERA-Interim (Figure 4a), the good MJO models (Figure 4b), the poor MJO models (Figure 4c), and the difference between the good and poor MJO models (Figure 4d). Similar to Figure 1, the good MJO models are much moister near the equator and slightly drier in off-equatorial regions, particularly in the Northern Hemisphere (Figure 4d), indicating much stronger meridional gradients in the mean low-level specific humidity near the MC in the good MJO models than the poor MJO models (cf. density in contours in Figure 4b and 4c). Significant differences in the zonal mean moisture gradient between the good and poor MJO models are also clearly evident in Figure 4. These discrepancies between good and poor MJO model moisture gradients over the MC are further supported by strong correlations between MJO propagation skill and the root-mean-square error (RMSE) of the zonal and meridional moisture gradients over the MC. Correlation coefficients of −0.65 and −0.72 are found between the MJO propagation skill and the RMSE of the zonal and meridional 650–900 hPa averaged winter mean specific humidity gradients, respectively. Figures 4a–4c also illustrate that the local mean low-level moisture over the MC tends to be maximized over large islands in both model simulations and ERA-Interim, suggesting land processes or circulations induced by land-sea contrasts contribute significantly to the high mean lower tropospheric moisture over the MC.

Figures 4e–4h illustrate meridional-vertical cross sections of the winter mean specific humidity over the MC region (averaged over 90°E–135°E) in ERA-Interim (Figure 4e), the good MJO models (Figure 4f), the poor MJO models (Figure 4g), and the difference between the good and poor MJO models (Figure 4h). In general, the observed meridional-vertical moisture profile is well represented in the good MJO models. The largest differences between good and poor MJO models are in the lower troposphere between 500 and 900 hPa, with more moisture near the equator and less moisture off of the equator (Figure 4h). Again, the difference in the mean moisture in the boundary layer between good and poor MJO models is rather weak, in agreement with weak correlations between model skill for mean moisture pattern in the boundary layer and MJO propagation skill as illustrated in Figure 3.

4. Summary and Conclusions

Despite its critical role in bridging large-scale climate and weather extremes worldwide, the MJO remains poorly represented in state-of-the-art climate models. In particular, the systematic eastward propagation of the MJO along the equator is not realistically captured in most present-day GCMs. Recent observational and modeling studies suggest that horizontal MSE or moisture advection in the lower troposphere, specifically the seasonal mean low-level MSE (moisture) by the MJO anomalous winds, plays an essential role for the eastward propagation of the MJO [e.g., *Kiranmayi and Maloney*, 2011; *Kim et al*., 2014; *Nasuno et al*., 2015; *Hsu and Li*, 2012; *Adames and Wallace*, 2015; *Jiang,* 2017].

Motivated by these studies and taking advantage of multimodel output from the recent MJOTF/GASS MJO evaluation project, we investigated the relationship between model skill in representing the lower tropospheric moisture over the Indo-Pacific region and MJO propagation skill across more than 20 GCM simulations. Significant correlations between model skill for the eastward propagation of the MJO and the November–April mean moisture pattern over the Indo-Pacific region are evident with maximum correlations in the lower troposphere between 650 hPa and 900 hPa and minimal correlations in the boundary layer. More specifically, model skill of the 650–900 hPa averaged mean specific humidity over the MC region exhibits a very high correlation (0.8) with model skill of the eastward propagation of the MJO, suggesting that realistic simulations of the mean low-level moisture pattern over the MC could be critical for realistic simulations of the eastward propagation of the MJO. While the observed mean low-level moisture maxima over the MC region are well-simulated in the good MJO models, they are greatly underestimated in the poor MJO models, leading to weaker horizontal mean moisture gradients and thus discrepancies in the horizontal moisture advection associated with the MJO. Results from this study further support the importance of horizontal MSE or moisture advection for the eastward propagation of the MJO based on multimodel simulations. These results also suggest that the seasonal mean lower tropospheric moisture pattern, particularly over the MC, can serve as an important diagnostic metric to evaluate MJO propagation in climate models.

Specific physical processes responsible for the model deficiencies in the mean low-level moisture pattern in the poor MJO models need to be further investigated. They could be associated with model deficiencies in

accurately simulating vertical mixing processes in the boundary layer, shallow cumulus clouds [*Cai et al*., 2013], large-scale moisture convergence associated with ascending motion within the Walker circulation, or the vigorous diurnal cycle over the MC region [e.g., *Love et al*., 2011; *Peatman et al*., 2014]. The close relationship between the mean moisture pattern over the MC and the MJO eastward propagation is also in general agreement with previous studies that have emphasized the role of the MC region for climate mean state and variability [*Neale and Slingo*, 2003; *Slingo et al*., 2003].

Moreover, even though we have mainly focused on the influences of the mean lower tropospheric moisture on the eastward propagation of the MJO, upscale feedbacks of the MJO to the mean moisture distribution remains an intriguing topic for future investigation, particularly over the MC region. More generally, we need to improve our understanding of the role of multiscale convective activity, including mesoscale convective systems, the local diurnal cycle, synoptic waves, and the MJO, in shaping the mean moisture pattern over the MC. The upcoming field campaign, "The Years of the Maritime Continent (YMC)" (A scientific plan of the YMC field campaign is available at the following link: www.jamstec.go.jp/ymc/docs/YMC_SciencePlan_v2.pdf), would provide an unprecedented opportunity to understand detailed multiscale interactive processes near the MC and thus help reduce the aforementioned model deficiencies in the mean moisture pattern.

Appendix A

Table A1 displays a summary of the 23 GCM simulations used in this study from the climate simulation component of the MJOTF/GASSMJO global model comparison project. It includes model acronym, full model name or institute, horizontal resolution, and number of vertical levels.

Table A1. Summary of the GCM Simulations[a]

Model Acronym	Full Model Name or Institution	Horizontal Resolution, Number of Levels
ACCESS1	Australian Community Climate and Earth System Simulator 1	1.875° × 1.25°, L85
BCCAGCM2.1	Beijing Climate Center Atmospheric GCM 2.1	T42 (2.8°), L26
CAM5	National Center for Atmospheric Research Community Atmosphere Model 5	1.25° × 0.9°, L30
CAM5-ZM	Lawrence Livermore National Laboratory CAM5	1.25° × 0.9°, L30
CanCM4^{+}	Canadian Centre for Climate Modelling and Analysis Coupled Model 4	2.8°, L35
CFS2	National Center for Environmental Prediction Climate Forecast System 2	T126 (1°), L64
CNRM-AM	Centre National de la Recherche Météo-France—ARPEGE Model	T127 (1.4°), L31
CNRM-CM	CNRM—Coupled Model	T127 (1.4°), L31
CNRM-ACM	CNRM - ARPEGE Coupled with MOCAGE	T127 (1.4°), L31
CWS-GFS	Taiwan Central Weather Bureau—Global Forecast System	T119 (1.4°), L40
EC-Earth	Swedish Meteorological and Hydrological Institute Rossby Centre Climate Model	T255 (80 km), L91
EC-GEM	Environment Canada—Global Environmental Multiscale Model	1.4°, L64
ECHAM5-SIT^{+}	Academia Sinica Taiwan (ECHAM coupled with SIT)	T63 (2°), L31
ECHAM6	Max Planck Institute for Meteorology	T63 (2°), L47
FGOALS-s2	Institute of Atmospheric Physics (Chinese Academy of Sciences)	R42 (2.8° × 1.6°), L26
GEOS5	Goddard Earth Observing System Model 5	0.625° × 0.5°, L72
GISS-E2	Goddard Institute for Space Studies—Model E2	2.5° × 2.0°, L40
ISUGCM	Iowa State University GCM	T42 (2.8°), L18
MIROC5	Model for Interdisciplinary Research on Climate 5	T85 (1.5°), L40
MRI-AGCM3	Meteorological Research Institute—Atmospheric-only GCM 3	T159, L48
NavGEM1	Navy Global Environmental Model 1	T359 (37 km), L42
SPCCSM3^{+}	Super-Parameterized Community Climate System Model 3	T42 (2.8°), L30
UCSD-CAM3	Scripps, University of California San Diego—CAM3	T42 (2.8°), L26

[a]Summary of the 23 GCM simulations used from the climate simulation component of the MJOTF/GASS experiment. Model acronym, full model name or institute, horizontal resolution, and number of model levels (preceded by L) are shown for each GCM simulation. Coupled GCM models are denoted with a plus-sign superscript. For horizontal resolution, spectral model wave number truncation (preceded by T for triangular and R for rhomboidal) and/or Gaussian grid spacing are shown.

Acknowledgments

We acknowledge the insightful comments from A. Adames and an anonymous reviewer. We thank modeling groups for making their model output available through the MJOTF/GASS MJO project. The multi-model output collected by this project and analyzed in this study is available for download at https://earthsystem-cog.org/projects/gassyotc-mip. We would also like to thank D. Waliser, E. Maloney, S. Ettammal, D. Baranowski, G. Cesana, and P. Ciesielski for their helpful discussions. This study is supported by the National Science Foundation (NSF) Climate and Large-Scale Dynamics Program under award AGS-1228302 and NOAA Climate Program Office under awards NA12OAR4310075, NA15OAR4310098, and NA15OAR4310177.

References

Adames, Á. F., and D. Kim (2016), The MJO as a dispersive, convectively coupled moisture wave: Theory and observations, *J. Atmos. Sci.*, *73*(3), 913–941, doi:10.1175/JAS-D-15-0170.1.

Adames, Á. F., and J. M. Wallace (2015), Three-dimensional structure and evolution of the moisture field in the MJO, *J. Atmos. Sci.*, *72*(10), 3733–3754, doi:10.1175/JAS-D-15-0003.1.

Andersen, J. A., and Z. Kuang (2012), Moist static energy budget of MJO-like disturbances in the atmosphere of a zonally symmetric aqua-planet, *J. Clim.*, *25*(8), 2782–2804, doi:10.1175/JCLI-D-11-00168.1.

Arnold, N. P., and D. A. Randall (2015), Global-scale convective aggregation: Implications for the Madden-Julian Oscillation, *J. Adv. Model. Earth Syst.*, *7*(4), 1499–1518, doi:10.1002/2015MS000498.

Benedict, J. J., M. S. Pritchard, and W. D. Collins (2015), Sensitivity of MJO propagation to a robust positive Indian Ocean dipole event in the superparameterized CAM, *J. Adv. Model. Earth Syst.*, *7*(4), 1901–1917, doi:10.1002/2015MS000530.

Cai, Q., G. J. Zhang, and T. Zhou (2013), Impacts of shallow convection on MJO simulation: A moist static energy and moisture budget analysis, *J. Clim.*, *26*(8), 2417–2431, doi:10.1175/JCLI-D-12-00127.

Chikira, M. (2014), Eastward-propagating intraseasonal oscillation represented by Chikira-Sugiyama parameterization. Part II: Understanding moisture variation under weak temperature gradient balance, *J. Atmos. Sci.*, *71*(2), 615–639, doi:10.1175/JAS-D-13038.1.

Dee, D. P., et al. (2011), The ERA-Interim reanalysis: Configuration and performance of the data assimilation system, *Q. J. R. Meteorol. Soc.*, *137*(656), 553–597, doi:10.1002/qj.828.

Ferranti, L., T. N. Palmer, F. Molteni, and E. Klinker (1990), Tropical-extratropical interaction associated with the 30–60 day oscillation and its impact on medium and extended range prediction, *J. Atmos. Sci.*, *47*(18), 2177–2199, doi:10.1175/1520-0469(1990)047(2177:TEIAWT)2.0.CO;2.

Holloway, C. E., and J. D. Neelin (2009), Moisture vertical structure, column water vapor, and tropical deep convection, *J. Atmos. Sci.*, *66*(6), 1665–1683, doi:10.1175/2008jas2806.1.

Hsu, P., and T. Li (2012), Role of the boundary layer moisture asymmetry in causing the eastward propagation of the Madden–Julian oscillation, *J. Clim.*, *25*(14), 4914–4931, doi:10.1175/JCLI-D-11-00310.1.

Huffman, G. J., R. F. Adler, D. T. Bolvin, G. Gu, E. J. Nelkin, K. P. Bowman, Y. Hong, E. F. Stocker, and D. B. Wolff (2007), The TRMM multisatellite precipitation analysis (TMPA): Quasi-global, multiyear, combined-sensor precipitation estimates at fine scales, *J. Hydrometeorol.*, *8*, 38–55, doi:10.1175/JHM560.1.

Hurrell, J., G. A. Meehl, D. Bader, T. L. Delworth, B. Kirtman, and B. Wielicki (2009), A unified modeling approach to climate system prediction, *Bull. Am. Meteorol. Soc.*, *90*(12), 1819–1832, doi:10.1175/2009BAMS2752.1.

Jiang, X. (2017), Key processes for the eastward propagation of the Madden-Julian oscillation based on multi-model simulations, *J. Geophys. Res. Atmos.*, *122*, 755–770, doi:10.1002/2016JD025955.

Jiang, X., et al. (2015), Vertical structure and physical processes of the Madden-Julian oscillation: Exploring key model physics in climate simulations, *J. Geophys. Res. Atmos.*, *120*, 4718–4748, doi:10.1002/2014JD022375.

Jiang, X., M. Zhao, E. D. Maloney, and D. E. Waliser (2016), Convective moisture adjustment time scale as a key factor in regulating model amplitude of the Madden-Julian oscillation, *Geophys. Res. Lett.*, *43*, 10,412–10,419, doi:10.1002/2016GL070898.

Kim, D., J.-S. Kug, and A. H. Sobel (2014), Propagating versus nonpropagating Madden–Julian oscillation events, *J. Clim.*, *27*(1), 111–125, doi:10.1175/JCLI-D-13-00084.1.

Kiranmayi, L., and E. D. Maloney (2011), Intraseasonal moist static energy budget in reanalysis data, *J. Geophys. Res.*, *116*, D21117, doi:10.1029/2011JD016031.

Klingaman, N. P., X. Jiang, P. K. Xavier, J. Petch, D. Waliser, and S. J. Woolnough (2015), Vertical structure and physical processes of the Madden-Julian oscillation: Synthesis and summary, *J. Geophys. Res. Atmos*, *120*, 4671–4689, doi:10.1002/2015JD023196.

Love, B. S., A. J. Matthews, and G. M. S. Lister (2011), The diurnal cycle of precipitation over the Maritime Continent in a high-resolution atmospheric model, *Q. J. R. Meteorol. Soc.*, *137*(657), 934–947, doi:10.1002/qj.809.

Madden, R. A., and P. R. Julian (1971), Detection of a 40–50 day oscillation in the zonal wind in the tropical Pacific, *J. Atmos. Sci.*, *28*(5), 702–708, doi:10.1175/1520-0469(1971)028(0702:DOADOI)2.0.CO;2.

Madden, R. A., and P. R. Julian (1972), Description of global-scale circulation cells in the tropics with a 40–50 day period, *J. Atmos. Sci.*, *29*(6), 1109–1123, doi:10.1175/1520-0469(1972)029(1109:DOGSCC)2.0.CO;2.

Maloney, E. D. (2009), The moist static energy budget of a composite tropical intraseasonal oscillation in a climate model, *J. Clim.*, *22*(3), 711–729, doi:10.1175/2008JCLI2542.1.

Maloney, E. D., and M. J. Dickinson (2003), The intraseasonal oscillation and the energetics of summertime tropical western North Pacific synoptic-scale disturbances, *J. Atmos. Sci.*, *60*(17), 2153–2168, doi:10.1175/1520-0469(2003)060<2153:TIOATE>2.0.CO;2.

Maloney, E. D., and A. H. Sobel (2004), Surface fluxes and ocean coupling in the tropical intraseasonal oscillation, *J. Clim.*, *17*(22), 4368–4386, doi:10.1175/JCLI-3212.1.

NAS (2016), *Next Generation Earth System Prediction: Strategies for Subseasonal to Seasonal Forecasts*, Natl. Res. Council, Natl. Acad. of Sci., 290 pp., Washington, D. C., doi:10.17226/21873.

Nasuno, T., T. Li, and K. Kikuchi (2015), Moistening processes before the convective initiation of Madden–Julian oscillation events during the CINDY2011/DYNAMO period, *Mon. Weather Rev.*, *143*(2), 622–643, doi:10.1175/MWR-D-14-00132.1.

Neale, R., and J. Slingo (2003), The Maritime Continent and its role in the global climate: AGCM study, *J. Clim.*, *16*(5), 834–848, doi:10.1175/1520-0442(2003)016(0834:TMCAIR)2.0.CO;2.

Neena, J. M., J. Y. Lee, D. Waliser, B. Wang, and X. Jiang (2014), Predictability of the Madden–Julian oscillation in the intraseasonal variability hindcast experiment (ISVHE), *J. Clim.*, *27*(12), 4531–4543, doi:10.1175/JCLI-D-13-00624.1.

Peatman, S. C., A. J. Matthews, and D. P. Stevens (2014), Propagation of the Madden-Julian oscillation through the Maritime Continent and scale interaction with the diurnal cycle of precipitation, *Q. J. R. Meteorol. Soc.*, *140*(680), 814–825, doi:10.1002/qj.2161.

Petch, J., D. Waliser, X. Jiang, P. Xavier, and S. Woolnough (2011), A global model intercomparison of the physical processes associated with the MJO, GEWEX News, August, 3 pp.

Pritchard, M. S., and C. S. Bretherton (2014), Causal evidence that rotational moisture advection is critical to the superparameterized Madden–Julian oscillation, *J. Atmos. Sci.*, *71*(2), 800–815, doi:10.1175/JAS-D-13-0119.1.

Raymond, D. J. (2000), Thermodynamic control of tropical rainfall, *Q. J. R. Meteorol. Soc.*, *126*(564), 889–898, doi:10.1002/qj.49712656406.

Raymond, D. J., and Ž. Fuchs (2009), Moisture modes and the Madden–Julian oscillation, *J. Clim.*, *22*(11), 3031–3046, doi:10.1175/2008JCLI2739.1.

Slingo, J., P. Inness, R. Neale, S. Woolnough, and G. Y. Yang (2003), Scale interactions on diurnal to seasonal timescales and their relevance to model systematic errors, *Ann. Geophys.*, *46*(1), 139–155, doi:10.4401/ag-3383.

Sobel, A., and E. Maloney (2012), An idealized semi-empirical framework for modeling the Madden–Julian oscillation, *J. Atmos. Sci.*, *69*(5), 1691–1705, doi:10.1175/JAS-D-11-0118.1.

Sobel, A., and E. Maloney (2013), Moisture modes and the eastward propagation of the MJO, *J. Atmos. Sci.*, *70*(1), 187–192, doi:10.1175/JAS-D-12-0189.1.

Sobel, A., S. Wang, and D. Kim (2014), Moist static energy budget of the MJO during DYNAMO, *J. Atmos. Sci.*, *71*(11), 4276–4291, doi:10.1175/JAS-D-14-0052.1.

Sobel, A. H., E. D. Maloney, G. Bellon, and D. M. Frierson (2010), Surface fluxes and tropical intraseasonal variability: A reassessment, *J. Adv. Model. Earth Syst.*, *2*(1), doi:10.3894/JAMES.2010.2.2.

Vitart, F., et al. (2012), Subseasonal to seasonal prediction: Research implementation plan, WWRP/THORPEX-WCRP Report, 3 pp.

Waliser, D. E., et al. (2012), The "year" of tropical convection (May 2008–April 2010): Climate variability and weather highlights, *Bull. Am. Meteorol. Soc.*, *93*(8), 1189–1218, doi:10.1175/2011BAMS3095.1.

Wang, B. (2012), *Intraseasonal Variability in the Atmosphere-Ocean Climate System*, Second, chap. Theories, 335-398 ed., edited by W. K. M. Lau and D. E. Waliser, 613 pp., Springer, Berlin.

Wolding, B. O., E. D. Maloney, and M. Branson (2016), Vertically resolved weak temperature gradient analysis of the Madden-Julian oscillation in SP-CESM, *J. Adv. Model. Earth Syst.*, doi:10.1002/2016MS000724.

Zhang, C. (2013), Madden-Julian oscillation: Bridging weather and climate, *Bull. Am. Meteorol. Soc.*, *94*(12), 1849–1870, doi:10.1175/BAMS-D-12-00026.1.

Zhang, C. D. (2005), Madden-Julian oscillation, *Rev. Geophys.*, *43*, RG2003, doi:10.1029/2004RG000158.